

High Lift Force with 275 Hz Wing Beat in MFI

E. Steltz, S. Avadhanula, and R.S. Fearing

Department of EECS, University of California, Berkeley, CA 94720

{ees132 srinath ronf} @eecs.berkeley.edu

Abstract—The Micromechanical Flying Insect (MFI) project aims to create a 25 mm (wingtip to wingtip) flapping wing micro air vehicle inspired by the aerodynamics of insect flight. A key challenge is generating appropriate wing trajectories. Previous work [1] showed a lift of 506 μN at 160 Hz using feedforward control. In this paper, refinements to the MFI design including those in [2] increased wing beat frequency to 275 Hz and lift to 1400 μN using pure sinusoidal drive for a fixed benchtop experiment. We show through simplified aerodynamic models that not only do sinusoidal actuator drives produce close to maximal lift, but significantly improved wing trajectories due to non-sinusoidal actuator drives are practically unobtainable due to actuator limitations.

I. INTRODUCTION

A flapping indoor micro air vehicle is an attractive proposition for its miniature size, ability to maneuver aggressively and hovering capability. The Micromechanical Flying Insect (MFI) at UC Berkeley (current prototype in Fig. 1) has been under development since 1998 to fulfill such a role. For each of its two wings, it utilizes two piezoelectric bending actuators [3] whose displacement is amplified through a double fourbar mechanism and a differential to create a flapping and rotational degree of freedom. The current version of the MFI fourbar/differential thorax is shown in Fig. 2.



Fig. 1. Current two wing, 4DOF MFI.

Previous versions of the MFI transmission mechanism have produced lift forces up to 506 μN [1] from a single wing. However, this lift is marginal considering the target weight of the MFI (1000 μN). To improve lift forces, several design changes were made to increase the resonant frequency

and general behavior of the thorax. The result is a structure discussed in Section II which produced 1400 μN of lift from a single wing, well in excess of the required 500 μN .

In Section III-A, different methods of driving the resonant thorax to maximize lift force are explored. Considering the structural and actuator limitations, we attempt to optimize the lift force with respect to the constraints detailed in Section III-B.

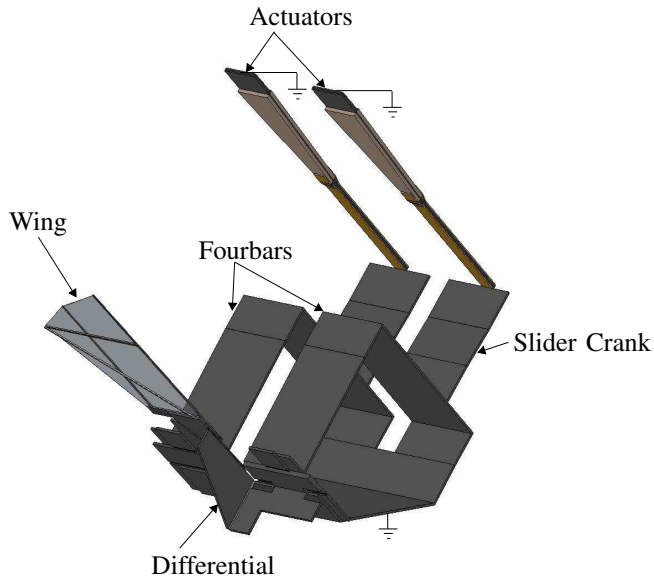


Fig. 2. MFI thorax

II. STRUCTURE 06- β

A. Structural Improvements

Considering the borderline lift of the 160Hz flapping mechanisms of the past, we take inspiration from honeybees to increase the lift force of the structure. Honeybee flight is characterized by high frequency (on the order of 250Hz) low amplitude (about 43 degrees) wing stroke for flight force generation [4]. Lift forces are expected to rise as the square of wing velocity (which is proportional to the product of flapping amplitude and frequency) [5]. The current stroke amplitude of the thorax is limited to 40 degrees (80 degrees total flap angle) due to plastic strain in the flexures. Flapping frequency, however, can be increased without significant flexure loading. The MFI thorax runs at resonance to maximize power transmission to the air; therefore the challenge is to increase the resonant frequency of the structure. However,

the damping of the wing flapping at higher frequency will be much higher, so power transmission to the wing also needs to be increased to keep the flapping amplitude high enough for proper stroke trajectory.

To increase the resonant frequency of the thorax, the wing inertia was reduced by utilizing a fabrication process that allows for carbon fiber wing spars (the previous spars were made of hollow polyimide tubing). This reduced the wing inertia from $17\text{mg}\cdot\text{mm}^2$ to $13\text{mg}\cdot\text{mm}^2$. Both wings are shown in Fig. 3. Since the wing inertia is the dominant inertia in the system, this can significantly increase the resonant frequency. The piezoelectric actuators' stiffness (the dominant stiffness in the system) was increased from 200 N/m to 400 N/m . Along with utilizing weight optimized fourbars and differential, the flapping frequency was increased from the previous reported value of 160 Hz in [1] to a new flapping frequency of 275 Hz .

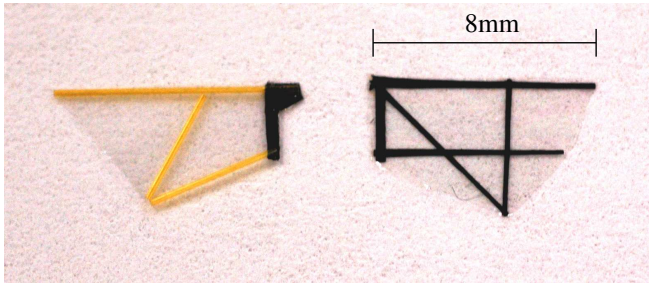


Fig. 3. Previous polyimide spar wing (left) and new carbon fiber spar wing (right).

To assure proper wing stroke amplitude, power losses in the structure must be minimized. The structure's flexure joints were optimized according to [2] to minimize joint power loss. At the time of this work, it was not known if the previously used miniature 10mg bimorph piezoelectric actuators had adequate power output; since the goal of this paper is not to test the actuators themselves, oversized, 100mg unimorph bending actuators were utilized so that power input to the system was not in question. Thus, the behavior of the thorax could be isolated without questioning the actuators. More recent work in [6] has further optimized and directly measured adequate power output from the 10mg bimorph actuators.

B. Lift Results

Structure $06-\beta$ appears in Fig. 4 on a precision weighing balance (model AAA-250L, Adam Equipment). A wind shield (white cardboard) was constructed to shield the weighing scale from the structure's thrust. Ground effects were minimized by spacing the wind shield at least one wing chord length below the wing.

As a first experiment, simple sine waves were used as input to the two oversized actuators driving structure $06-\beta$. Using only the phase difference between these sine waves and their amplitudes, the wing stroke was tuned manually to the profile of Fig. 5, graphically shown in Fig. 6. The

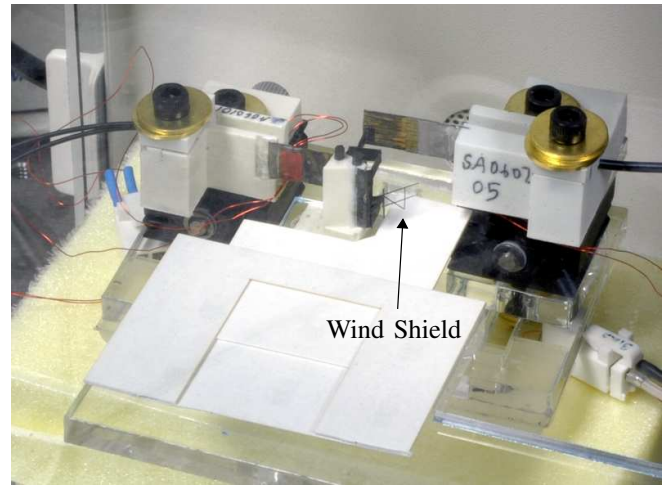


Fig. 4. Closeup of lift measurement setup for $06-\beta$.

target of this tuning was a constant 45 degree angle of attack through midstroke in addition to maximizing flapping angle and attempting to retain stroke symmetry, all occurring at the resonant frequency of the structure (275 Hz). Fig. 7 is a side view illustration of the wing stroke data of Fig. 5.

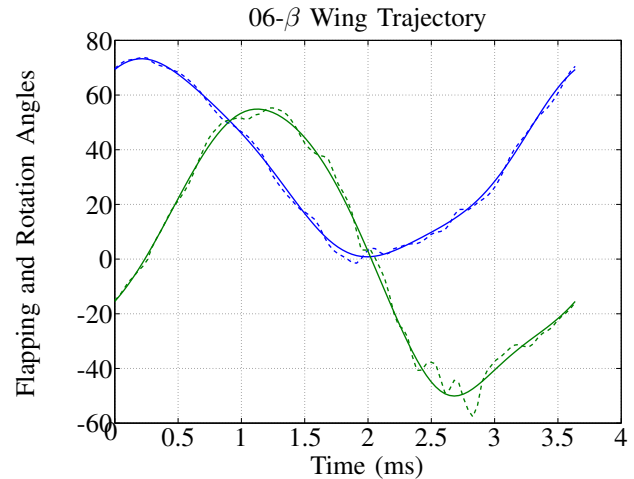


Fig. 5. Wing trajectory for $06-\beta$. Flapping angle is the top trace, rotation angle is the bottom. Raw data is plotted with a dotted line, filtered data with a solid line.

Three lift trials were run for the trajectory of Fig. 5, shown in Fig. 8. We measured an average mean lift of approximately $1400\ \mu\text{N}$, which is nearly three times the target lift value for a single wing.

III. OPTIMIZATION OF LIFT FORCE

Even though simple sine wave inputs to the system produced a significant amount of lift, other waveforms were explored to potentially improve lift forces. To formally begin this optimization process, all the limitations of the plant and actuators must be considered. Again, the plant referred to here is that of Fig. 2.

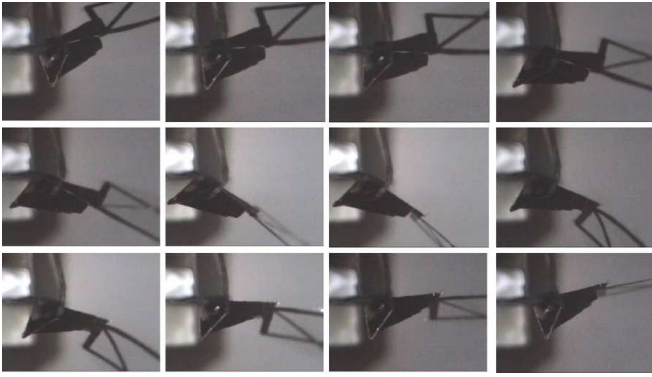


Fig. 6. Top view wing trajectory of 06- β .

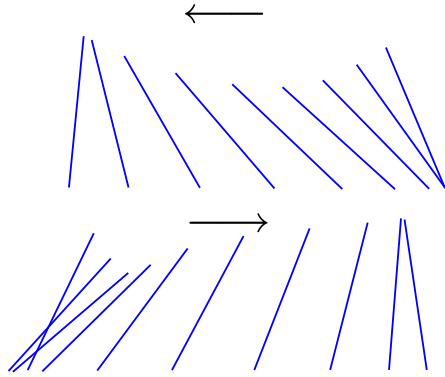


Fig. 7. Side view illustration of 06- β wingstroke.

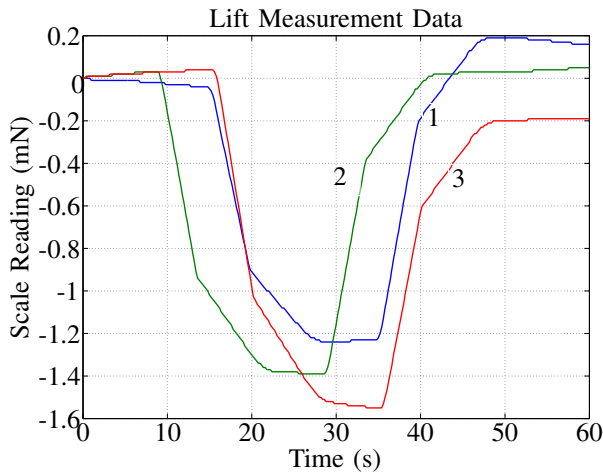


Fig. 8. Lift measurement data for 06- β .

A. Optimization Considerations

Several fundamental aspects of the plant dynamics govern the available control strategies for the system. Most are associated with the actuators; as mentioned earlier, for these lift maximization tests, we used oversized (about 100mg) piezoelectric unimorph actuators. The key limits are:

- **Actuator Force Saturation** - The most important aspect of the plant is the severe actuator saturation which typical feedback control problems usually do not encounter. Our composite PZT unimorph actuators are typically limited to voltages of about 200V. For this input level, they typically produce forces of around 200mN (with no displacement) and a free displacement of 400-500 μm . Beyond 200V, the actuators saturate, i.e, they do not produce significant additional force or displacement. Beyond about 300V, there is a risk of electrical breakdown across the PZT plate.
- **Actuator Dynamics** - The PZT unimorph actuators are used in a bending mode. Up to their first bending resonant mode, they behave well, but they rapidly begin to exhibit undesirable bending modes beyond their first bending resonance.
- **Poor behavior at high frequencies** - High frequency oscillatory modes arise if the complete system is driven with frequencies beyond approximately 1000Hz. Thus any allowable control system must restrict itself to producing actuations with frequency content below 1000Hz.
- **Periodic Motions** - Interesting flight trajectories have periodic motions in the range 150Hz-300Hz. Since the plant is not chaotic or naturally unstable, this implies that the input has to be periodic as well with the same base frequency as the desired output period.
- **Lift maximization** - Finally, overall lift production rather than the exact trajectory used to generate this lift is of interest. In other words, if two different trajectories produce equal lifts, we do not differentiate between them. As a long term problem, different trajectories must be analyzed to optimize system efficiency. However, for now, we only consider overall lift force production.

The aerodynamic model is given by [7]. This leads to one limitation of the optimization. The aerodynamic model of [7] is specialized for fruitfly flight (150Hz, 120 degrees of flapping). Structure 06- β flaps at 275Hz and 40 degrees of flapping amplitude, which leaves a considerable difference in the Reynolds number for the two cases and a possible loss of dynamic similarity. In fact, the aerodynamic model predicts a lift force of 740 μN for the trajectory of Fig. 5 where 1400 μN was measured. Although a revised high frequency, low stroke aerodynamic model would be ideal, we will assume that although the absolute magnitude of the lift force may not be accurate, the general aerodynamic trends will remain valid in the optimization procedure. Thus the best drive \mathbf{u} is:

$$\max_{\mathbf{u} \in \mathcal{P}_u} \bar{F}_L(\mathbf{u}) \quad (1)$$

where \mathcal{P}_u is the family of inputs that are possible given actuator and structural limitations and \bar{F}_L is the time averaged lift force.

B. Wing Drive Model

As stated earlier, only periodic system inputs that do not excite undesirable high frequency resonances of the structure are of interest. If the highest drive frequency component must remain below 1000Hz and the main drive frequency is up to 300Hz, the system input can be expressed generally as

$$u(t) = u_1 \sin \omega t + u_2 \sin 2\omega t + u_3 \cos 2\omega t + u_4 \sin 3\omega t + u_5 \cos 3\omega t \quad (2)$$

For now, actuator saturation will be ignored to optimize considering an ideal actuator. Some of the trajectory outputs of the optimization, therefore, might not be feasible, but could hint at design improvements to the structure. An additional assumption of a “perfect” differential was made, which means the two fourbar motions are completely dynamically uncoupled. This ideal differential acts purely kinematically to produce flapping and rotation from the two fourbar outputs. In other words, the simplified method shown in Fig. 9 was used to calculate lift force generated for a given input trajectory $u(t)$.

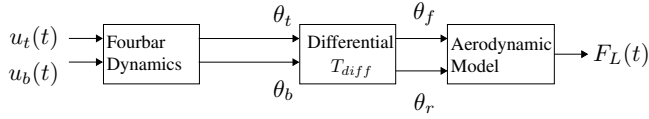


Fig. 9. Simplified model for calculating mean lift

We consider five separate families of inputs, using the conventions illustrated in Fig. 10. The angles of the top and bottom spar of the differential are denoted $\theta_{t,i}$ and $\theta_{b,i}$ respectively (equivalent to the output angles of the final fourbar links, which are attached to differential links 4 and 1 of Fig. 10) for the i^{th} trajectory. $\theta_{r,i}$ represents the rotation angle of the wing, which is attached to link 2. T_{diff} is a known nonlinear function that represents the relationship between the difference in the fourbar angular inputs ($\theta_{t,i} - \theta_{b,i}$) and the wing rotation $\theta_{r,i}$. A detailed analysis of the differential kinematics will not be presented here; the reader is referred to [8] for a complete analysis.

We consider 5 different distinct families of system behaviors and define them in terms of either the output or input trajectory.

C. Case 1

The first case will be the “best” case, taken as a maximum lift case from experiments by Dickinson [5] et. al. The flapping in Case 1 is forced to be a smoothed triangular wave while the rotation is forced to be a smoothed square wave. A triangular flapping trajectory implies that the flapping velocity is a smoothed square wave; a square wave rotation trajectory implies that the wing is maintained at the optimal angle of attack (45 degrees) for the majority of the wing stroke. The wing stroke is therefore defined by

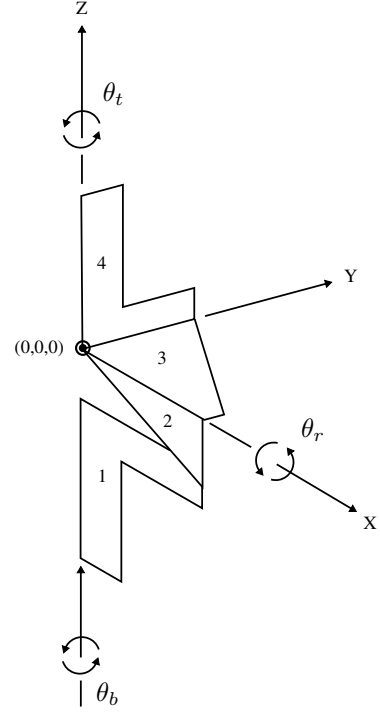


Fig. 10. Kinematic representation of the wing differential mechanism.

$$\theta_{t,1}(t) = \theta_0 (\cos \omega t + 1/9 \cos 3\omega t) \quad (3)$$

$$\theta_{r,1}(t) = \theta_{r,0} (\sin \omega t + 1/9 \sin 3\omega t) \quad (4)$$

$$\theta_{b,1}(t) = \theta_{t,1}(t) + T_{diff}^{-1}(\theta_{r,1}(t)) \quad (5)$$

Note that in this case, the torques required to drive the leading and lagging spars are unequal because $\theta_{t,1}(t) \neq \theta_{b,1}(t - \eta) \forall \eta$. In other words, the top and bottom spar trajectories are not simply different phases of the same trajectory.

D. Case 2

Next consider a slight variation of Case 1, where instead of directly forcing the rotation to be a certain trajectory, the top and bottom spars are the same trajectory but offset in time.

$$\theta_{t,2}(t) = \theta_0 (\cos \omega t + 1/9 \cos 3\omega t) \quad (6)$$

$$\theta_{b,2}(t) = \theta_{t,2}(t - 2\frac{20}{180\omega}) \quad (7)$$

$$\theta_{r,2}(t) = T_{diff}(\theta_{b,2}(t) - \theta_{t,2}(t)) \quad (8)$$

In other words, $\theta_{b,2}(t)$ is $\theta_{t,2}(t)$ delayed by 20° phase.

E. Case 3

In this case, the flapping and rotations are pure sinusoids:

$$\theta_{t,3}(t) = \theta_0 \cos \omega t \quad (9)$$

$$\theta_{r,3}(t) = \theta_{r,0} \sin \omega t \quad (10)$$

$$\theta_{b,3}(t) = \theta_{t,3}(t) + T_{diff}^{-1}(\theta_{r,3}(t)) \quad (11)$$

Like in Case 1, the torques for the top and bottom spars are unequal because the trajectories of the spars are not simply offset in phase.

F. Case 4

In this case, the same sinusoidal trajectory is used for both the top and bottom spars, but they are delayed in phase to achieve rotation.

$$\theta_{t,4}(t) = \theta_0 \cos \omega t \quad (12)$$

$$\theta_{b,4}(t) = \theta_{t,4}(t - 2\frac{20}{180\omega}) \quad (13)$$

$$\theta_{r,4}(t) = T_{diff}(\theta_{b,4}(t) - \theta_{t,4}(t)) \quad (14)$$

In this case, the torque on both the top and bottom spars are equal but delayed in phase.

G. Case 5

Lastly, instead of actively trying to achieve any specific wing trajectory, simple sinusoidal drives are used on the two actuators. The dynamics of the system take these simple sinusoids into a periodic trajectory. The two actuators are driven out of phase and generate the rotation from the difference of the two fourbar outputs.

$$u_{t,5}(t) = u_0 \cos \omega t \quad (15)$$

$$u_{b,5}(t) = u_0 \cos \omega(t - t_u) \quad (16)$$

The dynamics of the fourbar are then solved to find the trajectories of the top and bottom spars of the fourbar. These trajectories will, in general, have higher harmonic content due to the nonlinearities in the fourbar. Since an ideal differential has been assumed (no coupling between the fourbar outputs), the top and bottom spar trajectories will be related by

$$\theta_{b,5}(t) = \theta_{t,5}(t - t_u) \quad (17)$$

and the wing rotation follows as:

$$\theta_{r,5} = T_{diff}(\theta_{b,5}(t) - \theta_{t,5}(t)) \quad (18)$$

The specific kinematic and dynamic parameters used in the optimization simulations are omitted here, but can be found in [8]. A visualization of the trajectories in the 5 cases appear in Figs. 11 and 12.

If the output trajectories in cases 1-4 are used to solve the dynamic model for the inputs (and for case 5 simply run the dynamic model forward) while considering the aerodynamic model, the lift force trajectories of Fig. 13 and the mean forces summarized in Table I are produced. The input trajectories to the two actuators are also plotted in Fig. 14.

TABLE I

PREDICTED MEAN LIFT OBTAINED BY VARIOUS TRAJECTORIES.

Trajectory	1	2	3	4	5
Mean lift (μN)	919	782	830	786	867
Req. Actuator Voltage (V)	1110	1110	240	240	220

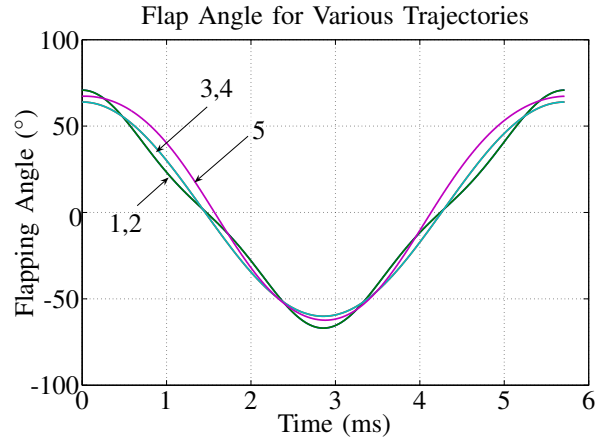


Fig. 11. Comparison of flapping angle obtained in the five trajectories.

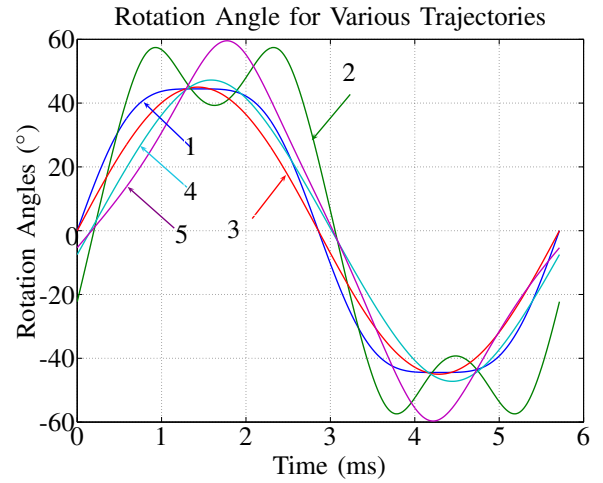


Fig. 12. Comparison of rotations obtained with the four trajectories.

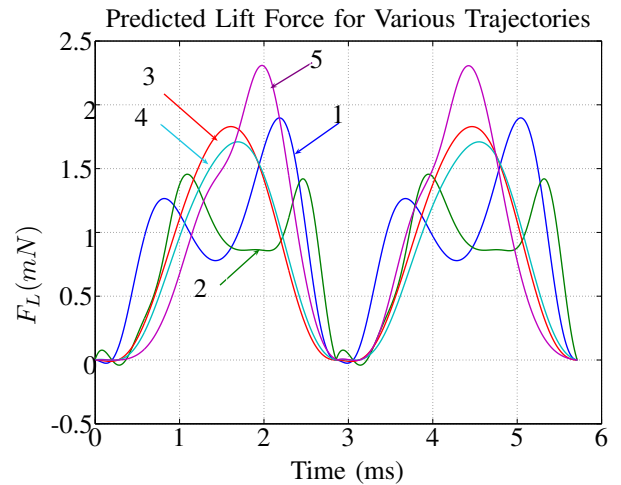


Fig. 13. Comparison of predicted lift forces obtained from various trajectories.

Several interesting observations can be made from these simulation results. First, one immediately notices that the inputs shown in Fig. 14 for cases 1 and 2 are well above

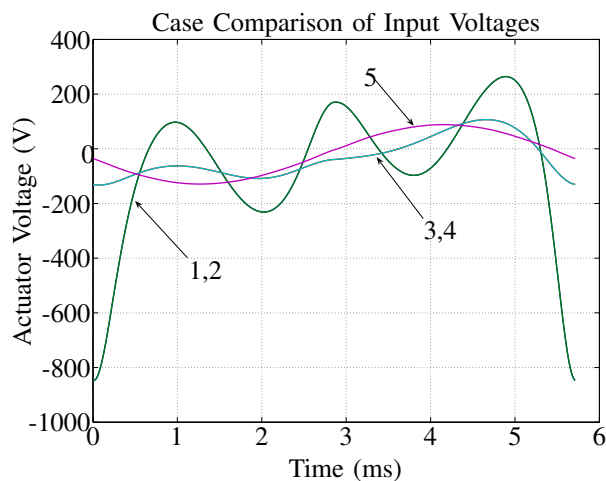


Fig. 14. Comparison of input voltages required for various trajectories.

the available saturation limits of the actuator and are therefore not feasible. Besides this point, these trajectories only produce about a 6% increase in mean lift at the cost of a five-fold increase in the required input actuation. Combined with superior lift production with less input effort than in cases 3 and 4, this analysis presents a convincing case for higher harmonic content not being necessary in the actuator input waveforms. The authors would like to note that this conclusion is drawn only for our structure given the available piezoelectric technology and plant dynamics; this conclusion might not be true for all flapping wing transmissions. In fact, it is true that actuator inputs with higher harmonic content can produce higher mean lift forces. This being said, the best drive scenario for the specific structure detailed in this paper is case 5 - simple sine waves with a phase difference as the input to the piezoelectric actuators. Again, this does not mean that the output trajectory only has the main mode for its frequency content; fourbar nonlinearities in fact will introduce higher order modes naturally.

IV. CONCLUSION AND FUTURE WORK

We have explored several important issues regarding wing trajectories of a flapping micro air vehicle. Notably among these is with the given plant dynamics and actuator limitations, it is not desirable to drive the wing into a trajectory with higher harmonic content than the main drive frequency;

in fact it is counterproductive when considering the input power it would require and the small gain in lift force one achieves.

We have also presented an improved MFI thorax structure from what is presented in [1] with new flexure technology and a wing with less inertia. In combination with stiffer and oversized actuators, we created the structure 06- β , which produced 1400 μN of lift force. To the authors' knowledge, this is by far the most lift from a flapping wing structure of this scale ever to be produced. Future work includes scaling down the drive actuators while keeping them energetically capable of the same wing trajectory and repeating the lift result of 06- β . With the recent work in [6], the power density of 10mg bimorphs has been significantly improved, leading us to believe that takeoff using MFI technology is imminent. Our conjecture has recently been proven with the takeoff of a 60mg flapping air vehicle using MFI technology at Harvard [9].

V. ACKNOWLEDGMENTS

The authors would like to thank Prof. Robert Wood for numerous discussions regarding actuator and structure design.

REFERENCES

- [1] S. Avadhanula, R. Wood, E. Steltz, J. Yan, and R. Fearing, "Lift force improvements for the micromechanical flying insect," in *International Conference on Intelligent Robots and Systems*, Las Vegas, October 2003, pp. 1350–1356.
- [2] S. Avadhanula and R. Fearing, "Flexure design rules for carbon fiber microrobotic mechanisms," in *IEEE Int. Conf. on Robotics and Automation*, 2005.
- [3] R. J. Wood and E. Steltz, "Optimal energy density piezoelectric bending actuators," *Sensors and Actuators A*, vol. 119/2, pp. 476–488, 2004.
- [4] D. L. Altshuler, W. B. Dickson, J. T. Vance, S. P. Roberts, and M. H. Dickinson, "Short-amplitude high-frequency wing strokes determine the aerodynamics of honeybee flight," *PNAS*, vol. 102, pp. 18 213–18 218, 2005.
- [5] M. H. Dickinson, F.-O. Lehmann, and S. P. Sane, "Wing rotation and the aerodynamic basis of insect flight," *Science*, vol. 284, pp. 1954–1960, June 18 1999.
- [6] E. Steltz and R. Fearing, "Dynamometer power output measurements of piezoelectric actuators," in *IEEE Int. Conf. on Intelligent Robots and Systems*, 2007.
- [7] S. Sane and M. Dickinson, "The aerodynamic effects of wing rotation and a revised quasi-steady model of flapping flight," *J. of Exp. Biol.*, vol. 205, pp. 1087–1096, 2002.
- [8] S. Avadhanula, "Design, fabrication and control of the micromechanical flying insect," Ph.D. dissertation, University of California, Berkeley, 2006.
- [9] R. J. Wood, "Design, fabrication, and analysis of a 3dof, 3cm flapping wing mav," in *IEEE Int. Conf. on Intelligent Robots and Systems*, 2007.